Shaping of focal field with controllable amplitude, phase, and polarization

Jingjing Hao (郝晶晶), Zhongliang Yu (于忠良), Zhaozhong Chen (陈召忠), Hao Chen (陈 浩), and Jianping Ding (丁剑平)*

National Laboratory of Solid State Microstructures and School of Physics, Nanjing University, Nanjing 210093, China

**Corresponding author: jpding@nju.edu.cn*

Received March 18, 2014; accepted May 20, 2014; posted online August 23, 2014

We propose a method for configuring the distribution of amplitude, phase, and polarization in the focal region of vector beams. The polarization and phase of incident beam is spatially tailored so that it can produce a focal field that has elaborately prescribed shapes. Our work focuses on the design of a special focus structure with two oval rings, wherein a phase gradient and polarization gradient exist in the inner and outer rings, respectively. The incident light yielding the desired focal field is determined based on an iterative scheme involving vectorial diffraction calculations and fast Fourier transforms. Simulations and experiments demonstrate the generation of a focal field with phase and polarization gradients, which may find applications in optical manipulation.

OCIS codes: 050.1960, 260.5430, 120.5060.
doi: 10.3788/COL201412.090501.

The focusing of vector beams through high numerical aperture (NA) lenses has been the topic of much research because an elaborately designed focus can find applications in a variety of fields, including optical data storage, microscopy, material processing, near-field optics, micromechanics, and optical tweezers[1–10]. The common procedure for focus shaping is to configure the phase and/or amplitude profiles of an incident beam so that it yields the desired irradiance distribution in the focal volume. Recently, vector beams with space-variant polarization have drawn much attention as they are able to significantly influence the focusing behavior of light[11–14]. We have reported on the use of polarization-only modulation of incident beams to implement focus shaping[15], which demonstrates the functionality of polarization manipulation. On the other hand, it is well known that the tailoring of the wave-front (or phase profile) of light beam is preferred for the focus shaping because, normally, the phase plays a most important role in controlling the propagation behavior of light field; so we proposed to combine the modulation of the polarization and phase to realize more elaborate and versatile structuring of the focal field[16]. An iterative scheme for realizing a special polarization configuration in focus by simultaneous tailoring of both polarization and phase was reported. In this letter, we extend the study to the design of the vectorial focus that has simultaneously and independently modulated amplitude, phase, and polarization distribution of incident field. The specific shape (intensity, phase, and polarization) configurations in the focal field are achieved by optimizing the modulation of both the polarization and phase of the incident beams. The mathematical expressions of the focused fields are derived based on the vector diffraction theory, and numerical simulations and experimental measurements of tightly focused field intensity distributions are further demonstrated. The simulations and optical experiments on vectorial field shaping are performed to validate the feasibility of our method.

Any polarized vector field can be described by the combination of a pair of orthogonal components, which can be represented in circular polarization basis $\left(\hat{\mathbf{e}}_+, \hat{\mathbf{e}}_-\right)$ or in linear polarization basis $\left(\hat{\mathbf{e}}_x, \hat{\mathbf{e}}_y\right)$. The transformation between the two sets of base vectors are expressed in the following forms:

$$\hat{\mathbf{e}}_x = \frac{1}{\sqrt{2}}\left(\hat{\mathbf{e}}_+ + \hat{\mathbf{e}}_-\right), \quad \hat{\mathbf{e}}_y = -\frac{\mathrm{i}}{\sqrt{2}}\left(\hat{\mathbf{e}}_+ - \hat{\mathbf{e}}_-\right), \tag{1}$$

$$\hat{\mathbf{e}}_+ = \frac{1}{\sqrt{2}}\left(\hat{\mathbf{e}}_x + \mathrm{i}\hat{\mathbf{e}}_y\right), \quad \hat{\mathbf{e}}_- = \frac{1}{\sqrt{2}}\left(\hat{\mathbf{e}}_x - \mathrm{i}\hat{\mathbf{e}}_y\right). \tag{2}$$

Our endeavor starts with an inhomogeneous beam with random distributed amplitude, phase, and polarization across the cross section of beam, described as $A(x,y)e^{\mathrm{i}\phi(x,y)}\left[\cos\varphi(x,y)\hat{\mathbf{e}}_x + \sin\varphi(x,y)\hat{\mathbf{e}}_y\right]$, where $A(x, y)$, $\phi(x, y)$, and $\varphi(x, y)$, are the amplitude, phase retardation, and polarization angle of the incident light. Our aim is to optimize three parameters of the incident light by using an iterative scheme to create a desired polarization gradient and phase gradient structure in the focal volume. In this study, it is helpful to denote the incident field, $\bar{E}_0(x,y) = (E_+, E_-, E_z)^t$ (t denoting the transverse of matrix and $E_\pm = (E_x \pm \mathrm{i}E_y)/\sqrt{2}$), in the circular basis, as follows:

$$\begin{aligned}\vec{E}_0(x,y) &= A(x,y)e^{i\phi(x,y)}\left[\cos\varphi(x,y)\hat{\mathbf{e}}_x + \sin\varphi(x,y)\hat{\mathbf{e}}_y\right] \\ &= \frac{A(x,y)}{\sqrt{2}}\left[e^{i\alpha_+(x,y)}\hat{\mathbf{e}}_+ + e^{i\alpha_-(x,y)}\hat{\mathbf{e}}_-\right] \\ &= \frac{A(x,y)}{\sqrt{2}}\left(e^{i\alpha_+(x,y)}, e^{i\alpha_-(x,y)}, 0\right)^t, \end{aligned} \tag{3}$$

where $\alpha_+(x, y) = \phi + \varphi$ and $\alpha_-(x, y) = \phi - \varphi$. Equation (3) indicates that the locally linear polarization can be decomposed into a sum of the left- and right-hand circular polarization components each accompanied by their own phase profiles. As is well known, the phase profile of the light beam affects the propagation behavior of beam.

In the viewpoint of geometrical optics, the lens basically acts as a meridional redirector of the wave vectors of rays refracted at the lens, whereas it does not change the polarizations of a wave in the ray-accompanying coordinate frame[17]. As shown in Fig. 1, the direction of the refracted ray is given by spherical angles (θ, ϕ). The focusing transformation from the incident field $\vec{E}_0$ to the transmitted field $\vec{E}$ after the lens can be written in the operator form, $\vec{E}(\theta,\phi) = \hat{T}(\theta,\phi)\vec{E}_0$, where operator $\hat{T}$ consists of three successive geometrical rotations[18,19]: $\hat{T}(\theta,\phi) = \sqrt{\cos\theta}\hat{R}_z(-\phi)\hat{R}_y(-\theta)\hat{R}_z(\phi)$. Here $\sqrt{\cos\theta}$ is the apodization factor of the lens and $\hat{R}_n(\gamma)$ is the operator of the rotation of the coordinate frame about the n-axis by the angle γ, expressed by

$$\hat{R}_y(\gamma) = \begin{pmatrix} \cos\gamma & 0 & \sin\gamma \\ 0 & 1 & 0 \\ -\sin\gamma & 0 & \cos\gamma \end{pmatrix},$$
$$\hat{R}_z(\gamma) = \begin{pmatrix} \cos\gamma & \sin\gamma & 0 \\ -\sin\gamma & \cos\gamma & 0 \\ 0 & 0 & 0 \end{pmatrix}. \tag{4}$$

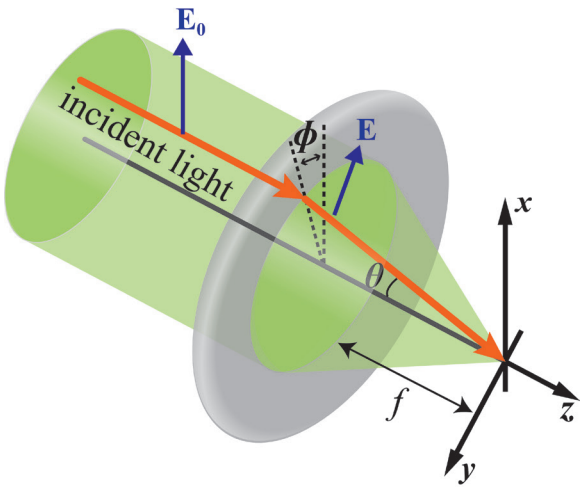

Fig. 1. Geometry of focusing system.

The three successive rotation operations describe the azimuthal rotation superimposing the x–z plane with the meridional plane of the local ray, the refraction through the lens on the angle θ therein, and the reverse rotation to the global coordinate frame. When applying to the field (E_+, E_-, E_z) in the circular basis, the transformation $\hat{T}$ acquires the following matrix form:

$$\hat{T}(\theta,\phi) = \sqrt{\cos\theta}\cdot\begin{pmatrix} a_1 & -a_2e^{-2i\phi} & \sqrt{2a_1a_2}e^{-i\phi} \\ -a_2e^{2i\phi} & a_1 & \sqrt{2a_1a_2}e^{i\phi} \\ -\sqrt{2a_1a_2}e^{i\phi} & -\sqrt{2a_1a_2}e^{-i\phi} & a_1 - a_2 \end{pmatrix}, \tag{5}$$

where $a_1 = \cos^2(\theta/2)$ and $a_2 = \sin^2(\theta/2)$.

The focal field of a monochromatic light beam passing through an aplanatic lens is calculated by the vectorial diffraction integral[17], which can also be written in terms of a Fourier transform (FT)[20,21]. For the sake of simplicity, we restrict our attention to the paraxial focusing in which the longitudinal component of the focal field can be omitted. If the tight focusing is necessitated, the longitudinal component must be taken into account and the triple components must be computed. On decomposing the circular polarization into a pair of orthogonal basis vectors, the left- and right-hand circular polarization components, the focal field at the point (x, y, z) with respect to the focus can be calculated by[16]

$$\begin{aligned} E_f(x,y,z) &= \begin{bmatrix} E_{f+}(x,y,z) \\ E_{f-}(x,y,z) \end{bmatrix} \\ &= \iint_S \hat{T}_2 \begin{bmatrix} A(x_0,y_0)e^{i\alpha_+(x_0,y_0)} \\ A(x_0,y_0)e^{i\alpha_-(x_0,y_0)} \end{bmatrix} \\ &\quad \times \exp\left[-i\frac{2\pi}{\lambda f}(xx_0 + yy_0)\right]dx_0dy_0, \end{aligned} \tag{6}$$

where (x_0, y_0) represents the exit pupil S of the lens, and $\hat{T}_2$ is the two-column counterpart of $\hat{T}$, expressed by

$$\hat{T}_2(\theta,\phi) = \sqrt{\cos\theta}\cdot\begin{pmatrix} a_1 & -a_2e^{-2i\phi} \\ -a_2e^{2i\phi} & a_1 \end{pmatrix}. \tag{7}$$

Equation (6) indicates that the focal field in a plane at a given axial position is obtained by a two-dimensional FT, which can be implemented efficiently on a computer with the help of algorithms such as the fast FT (FFT).

Our method simulates an iterative process between the forward and backward propagations that relates the incident and focal fields, which is analogous to the Gerchberg–Saxton (GS) algorithm for retrieving the phase of a pair of light distributions related via the FT[22]. The use of the GS algorithm in the implementation of our method allows for the fast shaping of the focal field. The flow chart of the iterative algorithm is depicted in Fig. 2. The iterative process starts with assuming a set of randomly distributed amplitude and

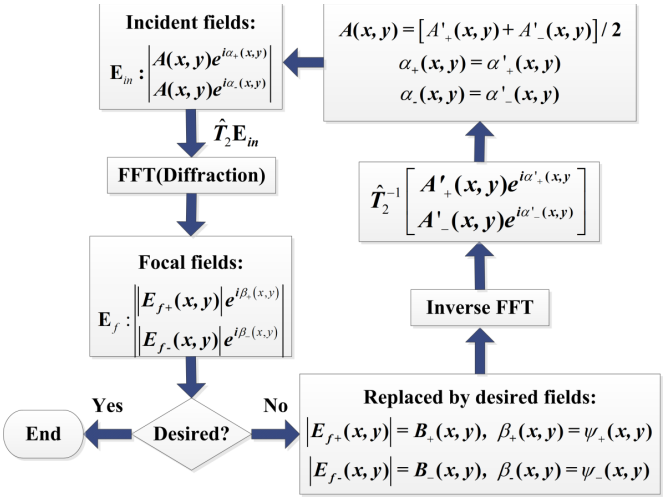

Fig. 2. Flow chart for iteratively searching for the optimal amplitude, phase, and polarization modulation of incident beam.

phase of the circular components of the incident beam (i.e., α_+ and α_- in Eq. (6) are uniform random numbers in [0, 2π], $A(x, y)$ is uniform random number in [0, 1]). The diffraction integrals in Eq. (6) are then calculated using the FFT, yielding the circular components of the field in the focal plane. Absolute values and phase values of the calculated components in the focal field are replaced by the ones of the prescribed polarization components $\left(B_+\exp(\mathrm{i}\psi_+), B_-\exp(\mathrm{i}\psi_-)\right)^t$. The renewed distribution in the incident beam is obtained through an inverse FFT by letting the reshaped focal field backward propagate to the entrance plane, where operator $\hat{T}_2^{-1}$ denotes the inverse of the matrix $\hat{T}_2$. We impose a constraint on the renewal process such that the incident field has two circular components with the amplitudes $A(x,y)=\left[A'_{i+}(x,y)+A'_{i-}(x,y)\right]/2$, while the phase values are left unchanged. The iterative search continues until a satisfactory focused field is found. In short, the iterative process optimizes two free parameters (i.e., the phase factors of the polarization components of the incident light, $\alpha_+$and α_-) to achieve the predetermined polarization components in the focal plane, which are represented by $\left(B_+\exp(\mathrm{i}\psi_+), B_-\exp(\mathrm{i}\psi_-)\right)^t$.

Once we obtain the mathematical expression for the incident light, we then need to build such a light field by the optical experiment. We have developed a method to generate vector beams with arbitrary space-variant distribution of polarization[23,24] and phase[25]. The experimental scheme is briefly outlined here (the detailed description of the optical system can be found in Ref. [23]). A 532-nm linear polarization light is input into the spatial light modulator (SLM)-based setup, giving rise to an output of the vector beams. The SLM (Holoeye Pluto with 1920 × 1080 pixels resolution), onto which a two-dimensional holographic grating pattern is written, splits the incident linearly polarized light into right- and left-hand circularly polarized components. Each of the two circularly polarized components acquires a specific phase factor from the diffraction of the holographic grating and a computer controls the specially designed holographic pattern to enable the dynamic generation of the space-variant linear polarization state and phase structure. Furthermore, additional amplitude modulation can be addressed with controlled modulation depth function. Now we utilize this optical system to create the vector beams that are optimally designed by the above-described iterative search. In order to visualize the designed focal field, the generated vector beams are focused by a lens with a focal length of 150 mm. The parameters of the focusing lens are chosen so that a CCD camera can detect a region-of-interest field in the focal plane, wherein a special polarization and intensity structure appears.

Here we present some special experimental results that can demonstrate the feasibility and capability of our method for pursuing the phase and polarization modulation in the focal field. We intend to configure a focal field that possesses space-variant polarization and phase distribution. Such a focal field can be useful for the optical manipulation. It is known that polarization and phase gradients give rise to the spin flow and orbital flow, respectively[19,26], which can result in opto-mechanical effects of light on the microscopic objects[27–29]. The focal field is designed such that it has a specific distribution of polarization and phase gradients. Figure 3 shows a double oval-shaped focus with specially designed polarization and phase structures, wherein the outer oval has a radial-variant polarization and the inner oval has a linearly x-polarized state and a helical phase. Figure 3(a) illustrates the polarization state in the focal plane. The simulated intensity and left- and right-circular polarized components are shown in Figs. 3(b)and (d). The phase of left- and right-circular polarized components are shown in Figs. 3(e) and (f). Note that the left- and right-circular components are set to the same helical phase of topological charge 1 within the inner oval stripe, which means that the resultant field in this region will have a scalar vortex with topological charge 1. As elaborated in Refs. [19, 26], the momentum density of optical field can be decomposed into two terms, which are referred to orbital flow density (OFD) and spin flow density (SFD), respectively. The OFD is calculated by $\vec{\mathbf{p}}_o=\mathrm{Im}\left(\vec{\mathbf{E}}^*\cdot\nabla\vec{\mathbf{E}}\right)$, the SFD is calculated by $\vec{\mathbf{p}}_s=\nabla\times\left[\mathrm{i}\cdot\left(\vec{\mathbf{E}}\times\vec{\mathbf{E}}^*\right)\right]$. The OFD is associated with phase gradient of the optical field and the SFD is associated with polarization gradient. The direction of OFD is identical with the phase gradient; however, the direction of SFD is orthogonal to the polarization gradient. After attaining the electric field distribution, the SFD and OFD of the focused field can be easily calculated and are plotted in Figs. 3(g) and (h), respectively. As shown in the figure, the OFD and SFD are spatially divided and concentrated in the inner and outer oval stripes, respectively, in which the blue arrowheads indicate the direction of each flow.

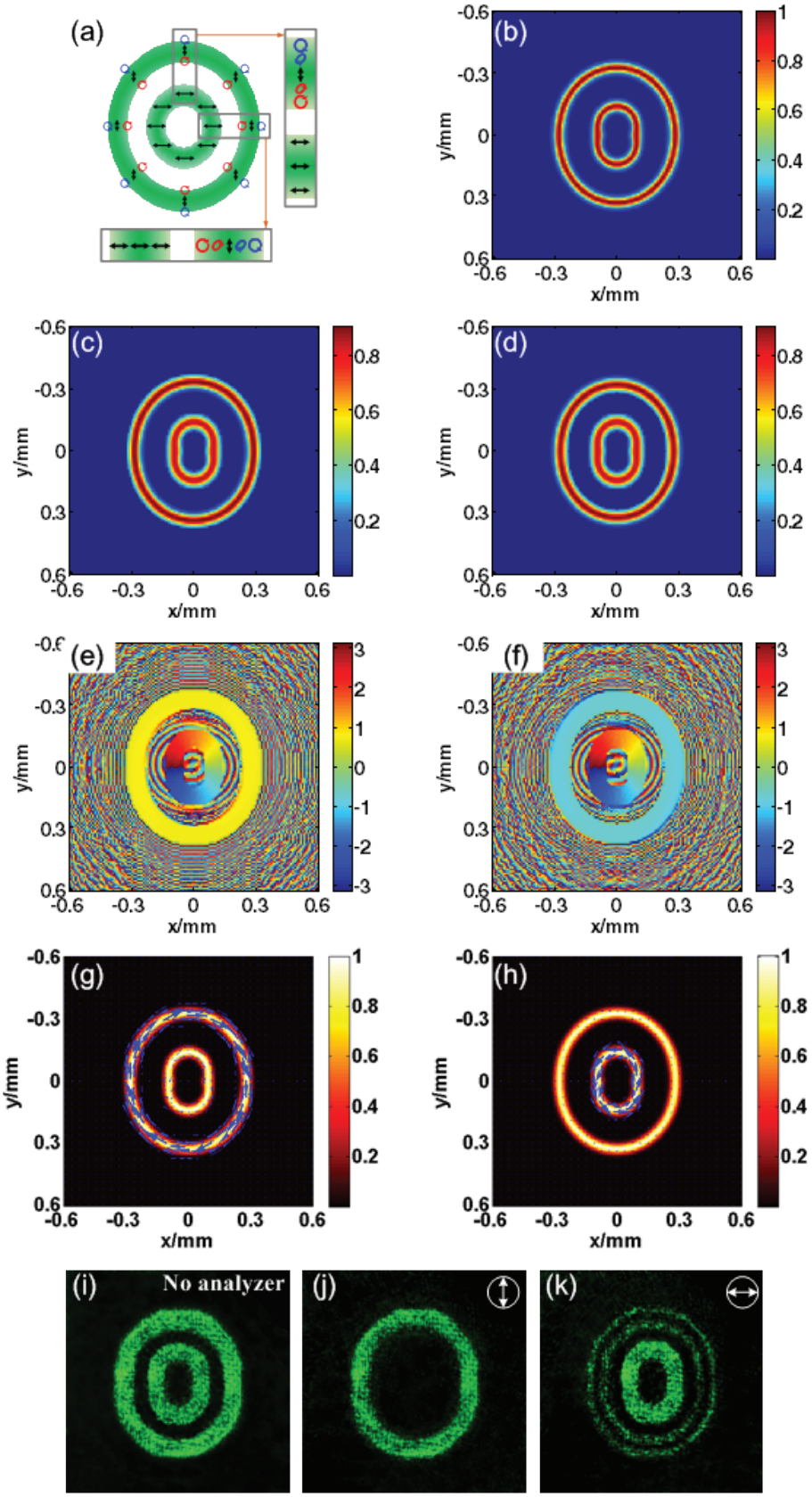

Fig. 3. Simulated and experimentally realized focal field with double oval-shape: (a) polarization state of the focal field, intensities of (b) total field, (c) right- and (d) left-circular components, phase structures of (e) right- and (f) left-circular components, and numerically calculated SFD and OFD in the focal field. The length of the arrows on the diagram indicates relative magnitude of the flow density. The intensity of the total field is shown in the background of each frame. (i) CCD recorded intensity of the focal field that is experimentally realized and intensities of the focal field after (j) horizontally and (k) vertically oriented polarizers.

Figure 3(a) indicates that the polarization state varies along the radial direction within the outer oval stripe, which gives rise to the azimuthal SFD confined in this region, as shown in Fig. 3(g). Meanwhile, Figs. 3(e) and (h) indicate that the inner oval stripe possesses a helical phase that is responsible for the azimuthal OFD shown in Fig. 3(h). The experimentally generated focal field is shown in Figs. 3(i)–(k), in which the intensity distribution with no analyzer and after being transmitted through the analyzer (whose orientation is indicated by the arrow) is demonstrated.

In conclusion, we demonstrate the possibility of generating focal fields with the controllable amplitude, phase, and polarization state. Furthermore, the spin and orbital flow in the focused field is manipulated independently. Our method provides a flexible way to tailor the optical field and thus helps us further explore engineering of vector beams targeted for specific applications of a high NA system, for example, in particles trapping and manipulation, which can benefit the investigation of the mechanic effect of vector beams.

This work was supported by the National Natural Science Foundation of China under Grant Nos. 11074116 and 11274158.

References

1. M. Gu, *Advanced Optical Imaging Theory* (Springer, Heidelberg, 2000).
2. L. E. Helseth, Opt. Commun. **212,** 343 (2002).
3. Z. Zhang, J. Pu, and X. Wang, Opt. Lett. **33,** 49 (2008).
4. D. G. Grier, Nature **424,** 810 (2003).
5. N. Sanner, N. Huot, E. Audouard, C. Larat**,** J. Huignard, and B. Loiseaux, Opt. Lett. **30,** 1479 (2005).
6. F. M. Dickey, S. C. Holswade, and D. L. Shealy, *Laser Beam Shaping Applications* (Taylor & Francis Group, Boca Raton, 2006).
7. I. Iglesias and B. Vohnsen, Opt. Commun. **271,** 40 (2007).
8. L. Guo, Z. Tang, C. Liang, and Z. Tan, Chin. Opt. Lett. **7,** 938 (2009).
9. K. A. Serrels, E. Ramsay, R. J. Warburton, and D. T. Reid, Nat. Photon. **2,** 311 (2008).
10. L. Guo, C. Min, S. Wei, and X. Yuan, Chin. Opt. Lett. **11,** 052601 (2013).
11. K. Huang, P. Shi, G. W. Cao, K. Li, X. B. Zhang, and Y. P. Li, Opt. Lett. **36,** 888 (2011).
12. Q. Zhan, Adv. Opt. Photon. **1,** 1 (2009).
13. S. N. Khonina and I. Golub, J. Opt. Soc. Am. A **29,** 1470 (2012).
14. K. Hu, Z. Chen, and J. Pu, Opt. Lett. **37,** 3303 (2012).
15. H. Chen, Z. Zheng, B. F. Zhang, J. Ding, and H. T. Wang, Opt. Lett. **35,** 2825 (2010).
16. J. Hao, Z. Yu, H. Chen, Z. Chen, H. Wang, and J. Ding, Appl. Opt. **53,** 785 (2014).
17. B. Richards and E. Wolf, Proc. R. Soc. Lond. A **253**, 358 (1959).
18. P.Torok, P. Higdon, and T. Wilson, Opt. Commun. **148,** 300 (1998).
19. A. Bekshaev, K. Bliokh, and M. Soskin J. Opt. **13,** 053001 (2011).
20. B. R. Boruah and M. A. A. Neil, Opt. Commun. **282,** 4660 (2009).
21. J. Lin, X.-C. Yuan, S. S. Kou, C. J. R. Sheppard, O. G. Rodríguez-Herrera, and J. C. Dainty, Opt. Lett. **36,** 1341 (2011).
22. R. W. Gerchberg and W. O. Saxton, Optik **35,** 237 (1972).
23. X. Wang, J. Ding, W. J. Ni, C. S. Guo, and H. T. Wang, Opt. Lett. **32,** 3549 (2007).
24. X. Wang, Y. Li, J. Chen, C. Guo, J. Ding, and H. T. Wang, Opt. Express **18,** 10786(2010).
25. H. Chen, J. Hao, B. F. Zhang, J. Xu, J. Ding, and H. T. Wang, Opt. Lett. **36,** 3179 (2011).
26. M. V. Berry, J. Opt. A: Pure Appl. Opt. **11,** 094001 (2009).
27. G. Cipparrone, I. Ricardez-Vargas, P. Pagliusi, and C. Provenzano, Opt. Express **18,** 6008 (2010).
28. Y. Roichman, B. Sun, Y. Roichman, J. Amto-Grill, and D. Grier, Phy. Rev. Lett. **100,** 013602 (2008).
29. D. Ruffner and D. Grier, Phys. Rev. Lett. **108,** 173602 (2012)